

Modelling and in-situ measurement of dynamic behavior of asphalt supporting layer in slab track system

Liu, Song; Chen, Xianhua; Ma, Yuewei; Yang, Jun; Cai, Degou; Yang, Guotao

DOI

[10.1016/j.conbuildmat.2019.116776](https://doi.org/10.1016/j.conbuildmat.2019.116776)

Publication date

2019

Document Version

Final published version

Published in

Construction and Building Materials

Citation (APA)

Liu, S., Chen, X., Ma, Y., Yang, J., Cai, D., & Yang, G. (2019). Modelling and in-situ measurement of dynamic behavior of asphalt supporting layer in slab track system. *Construction and Building Materials*, 228, Article 116776. <https://doi.org/10.1016/j.conbuildmat.2019.116776>

Important note

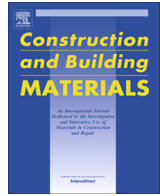
To cite this publication, please use the final published version (if applicable). Please check the document version above.

Copyright

Other than for strictly personal use, it is not permitted to download, forward or distribute the text or part of it, without the consent of the author(s) and/or copyright holder(s), unless the work is under an open content license such as Creative Commons.

Takedown policy

Please contact us and provide details if you believe this document breaches copyrights. We will remove access to the work immediately and investigate your claim.



Modelling and in-situ measurement of dynamic behavior of asphalt supporting layer in slab track system

Song Liu^a, Xianhua Chen^a, Yuewei Ma^b, Jun Yang^{a,*}, Degou Cai^c, Guotao Yang^d

^a School of Transportation, Southeast University, Nanjing 211189, China

^b Section of Railway Engineering, Faculty of Civil Engineering & Geoscience, Delft University Technology, Stevinweg 1, 2628 CN Delft, the Netherlands

^c Railway Engineering Research Institute, China Academy of Railway Sciences Corporation, Beijing 100081, China

^d China Railway Corporation, Beijing 100844, China

HIGHLIGHTS

- Application of asphalt supporting layer in slab track system.
- Dynamic responses of asphalt supporting layer under moving train load.
- In-situ measurement from practical railway line to validate the FE model.
- The optimal range of thickness of asphalt supporting layer for slab track system.

ARTICLE INFO

Article history:

Received 17 November 2018

Received in revised form 17 August 2019

Accepted 20 August 2019

Available online 27 August 2019

Keywords:

Slab track

Railway

Asphalt layer

Dynamic response

In-situ measurement

ABSTRACT

During the last decades, asphalt concrete has been introduced in both ballast and ballastless track (including but not limited to slab track) systems. The use of asphalt concrete provides better damping and waterproofing performance. For this reason, a supporting layer of asphalt concrete (ASL) was introduced to the latest Chinese slab track system. In this paper, an in-depth study of the dynamic behavior of ASL was presented using modelling and in-situ measurement approaches. In the FE model, the train load was simplified to be a time series of concentrated load on rail nodes, and asphalt concrete was modeled as viscoelastic material by Prony series. The FE model was validated against in-situ measurement on a test section, in which a monitoring system was setup during construction. A series of transient analysis were conducted to obtain the dynamic responses of ASL under moving train load. The parametric effects of thickness of ASL was also studied with respect to the dynamic responses of superstructure and substructure, as well as the stability and durability of ASL. The results showed that, under moving bogie load, the reach of the dynamic responses in ASL is about 7.5 m in the longitudinal direction, and the maximum values occur at the position beneath the rails. A thicker ASL is more favorable to ride comfort and structural stability of high-speed railway track system. However, considering the economic and construction factors, an optimal thickness range of 7–10 cm is suggested for ASL in CRTS III slab track.

© 2019 Elsevier Ltd. All rights reserved.

1. Introduction

Asphalt concrete, consisting of asphalt binder and mineral aggregates, is a composite material that has been widely used in asphalt pavement and runways, by virtue of its excellent carrying capacity and crack resistance. During the last decades, attempts have been made to introduce the asphalt concrete to the railway track system [1–5]. It was reported [6–10] that the well-designed asphalt concrete, as an alternative of the general track components (e.g. under-sleeper rail pads, sub-ballast layer, glued/bonded bal-

last, etc.), could sufficiently meet the requirements of strength and durability in the construction of both ballast track and ballast-less track (including but not limited to the slab track) systems.

For instance, in ballast track system, a sub-ballast layer of asphalt concrete has been successfully applied in Europe and USA to improve the drainage and to reduce the noise & vibration [4,11–15]. Regarding the application of asphalt concrete in the ballastless track system, it can be generally classified into three categories: (1) sleeper-anchored asphalt roadbed, (2) asphalt roadbed in slab track, and (3) asphalt waterproofing layer (See Fig. 1a) in slab track. Among them, the first two, which are developed in Germany and Japan respectively, are used to enhance the stability of

* Corresponding author.

E-mail address: yangjun@seu.edu.cn (J. Yang).

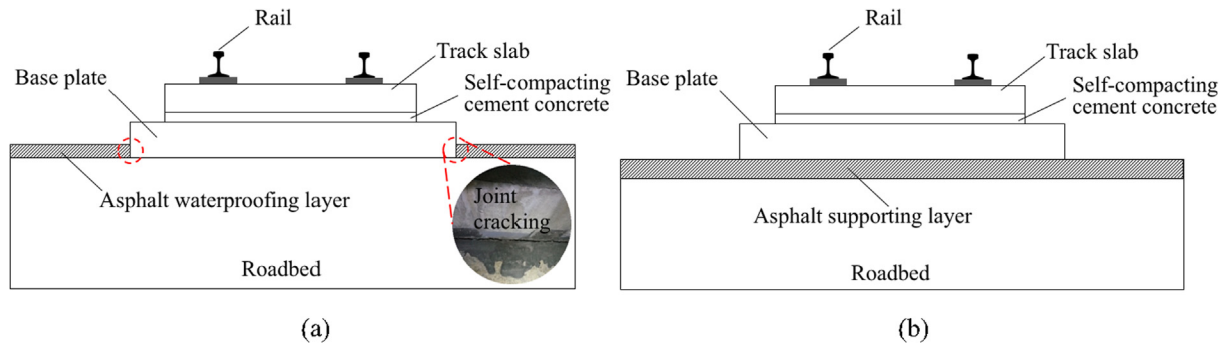


Fig. 1. Schematic graph of slab track system: (a) Application of asphalt waterproofing layer, (b) Application of asphalt supporting layer.

roadbed and reduce maintenance work. The last one (i.e. asphalt waterproofing layer), being paved on the shoulder of roadbed as shown in Fig. 1a, is mainly applied in the slab track systems of China [16]. Such a waterproofing layer of asphalt concrete is introduced to replace the traditionally favored layer of cement concrete, which tends to crack easily (as a result of the high thermal-induced stresses) and leads to water penetration & the freeze-thaw damage [17–19] consequently. The application of this asphalt waterproofing layer showed that the drainage performance of slab track system could be improved significantly [20] and the risk of the freeze-thaw damage could be minimized correspondingly. However, cracking and spalling damages (see Fig. 1(a)) are commonly observed at the interface between the concrete base plate and asphalt waterproofing layer. According to the report [17] of the field investigation, the cause of those damages might be attributed to the discontinuity of the layer of asphalt concretes.

To avoid the problem of the interface damages, a continuous & full-cross section asphalt layer (See Fig. 1b), as opposed to the discontinuous asphalt waterproofing layer, has been newly introduced and recently implemented in the latest CRTS III (the third type of China Railway Track System) slab track system [21]. To differentiate from the asphalt waterproofing layer mentioned before, this newly-introduced layer is named as “ASL”, following the abbreviation of “Asphalt Supporting Layer”. The newly coined terminology of “ASL” will be used throughout this paper. Also, it is worth noting that the latest CRTS III slab track system is developed from, and is thus quite similar to the former systems of CRTS I&II (i.e. the first and second types of China Railway Track System). The major difference among the CRTS track systems lies is the ASL and the self-compacting cement concrete layer, which are applied only in latest CRTS III slab track system. Due to the good viscoelasticity of the ASL and the high stiffness of the self-compacting cement concrete layer [22,23], it is expected that the performance of the latest CRTS III slab track system could be enhanced significantly.

However, as a newly-designed slab track system, this CRTS III system is still in the process of being tested. To check the applicability of this slab track system and further increase/promote its use in practice, there is still much work to be done, for instance,

- (1) Acquiring the knowledge about the dynamic behaviour of ASL: The dynamic behaviour of the ASL in the latest CRTS III slab track system, being subjected to the moving train load, is still unknown, although the viscoelasticity of ASL might presumably provide the slab track system good elasticity and damping. Accordingly, the assessment of the performance of the vehicle-track interaction, in terms of running stability, ride comfort, etc., is still in demand. In this study, a detailed modelling approach, namely finite element method, is used to study the dynamic responses of the ASL.

More details about the FE model of the interaction between the vehicle and the slab track are presented in Section 2.

- (2) Validating the FE model developed against in-situ measurement: The model without being verified/validated may generate subtle inaccuracy that being unnoticed can lead to wrong decisions [24]. To assess the validity of the FE model developed in this study, an in-situ measurement system has been devised and embedded into the test sections. These test sections as shown in Fig. 2a–b are constructed in the high-speed lines that are already in operation. More information about the setup of the measurements and the results of the experimental validation are presented in Section 3.
- (3) Identifying the proper parameter of the thickness of ASL: The choice of the thickness of ASL can not only affect the stiffness but also the damping of the track system. For example, in Japan, a thickness range of 15–20 cm was suggested for the construction of asphalt roadbed of Shinkansen lines, while in Germany the asphalt layer used in Getrac system is around 2 times thicker (i.e. 35 cm) than that of Japan [25]. To the best knowledge of the authors, there are no well-accepted values of the thickness of ASL, which should be determined depending on specific problems considered. Till now, the research on the identification of proper parameter of ASL, especially in the latest CRTS III slab track system, has not been performed adequately. More research attention on the importance of the thickness parameter of ASL has to be drawn.

For these reasons, it is aimed to perform an in-depth study on the dynamic behavior of ASL in the newly-designed (i.e. the latest CRTS III) slab track system, using the approaches of both numerical modelling and in-situ measurement. Through this study, it is expected to add the railway community the acquired knowledge about the application of asphalt concrete in slab track system. Also, the understanding of the dynamic behavior of ASL could be improved. Meanwhile, the proper values/ranges of the thickness of ASL, that will enhance the performance of vehicle-track interaction and ensure the high level of ride comfort by reducing the track vibration, could be suggested. The outcome of this study may guarantee, or at least contribute to, the smart design of the slab track system.

The structure of this paper is organized as follows. Firstly, a detailed description of FE model of slab track under the moving train load is presented in Section 2. Next, the accuracy of the FE model is demonstrated in Section 3 through a well-designed experimental validation against the in-situ measurements. Using the validated FE model, the dynamic responses of ASL under the moving train load are analyzed, and the results of the analyses are presented in Section 4. Following that, the effects of ASL thickness on the dynamic responses of superstructure and substructure were



Fig. 2. The asphalt supporting layer (ASL) in test section: (a) Under construction, (b) In operation.

studied in Section 5, wherein the choice of ASL thickness is discussed. Finally, concluding remarks are drawn in Section 6.

2. FE model description

In this section, the FE model of the interaction between the vehicle and the CRTS III slab track is presented. This FE model is developed in commercial computer program of ANSYS [26]. Also, ANSYS Parametric Design Language (APDL) is used to parameterize the FE model developed and to automate the common tasks.

Fig. 3(a) shows the structural design of the latest CRTS III slab track in the cross-sectional view. Using these geometrical information, which are adopted from China Code for Design of High-Speed Railway [27], the three-dimensional (3D) FE model (See Fig. 3(b)) of the CRTS III slab track is developed. It should be noted that, only a single track with two rails, instead of double tracks, is modeled by taking advantage of the symmetric characteristic of the slab track system.

In the 3D FE model, there are three slabs with an overall length of 16.8 m modeled. Such a length of three slabs is sufficient to minimize the boundary effects on the dynamic responses (i.e., acceleration, displacement and stress levels) in the middle cross-section of the middle slab that is of high interest for this study.

The UIC 60 rail is modeled as 2-Dimensional beam elements (BEAM188). The WJ-8 fastening system was simplified to be a spring-damper element (COMBIN14), and the interval of fastenings is 0.63 m. Apart from the rail and the fastening system, the other track components are all modeled as 8-node solid elements.

2.1. Non-reflective boundary conditions

In the longitudinal direction, the slab track is usually assumed to behave as an infinite continuum. However, due to the limitations of available computation resources, usually only a certain length of slab track structure is modelled in numerical simulation, and various methods are utilized to eliminate the effects of the boundaries (these boundaries do not exist in the real structure), such as boundary element method, infinite element method, and artificial boundary conditions. In this study, the non-reflective boundary conditions is adopted, which is a type of artificial boundary conditions that enables vibration wave propagates towards the far-field area and prevents the reflection of outward propagating waves back into the model.

In this study, the non-reflective boundary conditions, which enables vibration wave propagates towards the far-field area and prevents the reflection of outward propagating waves back into

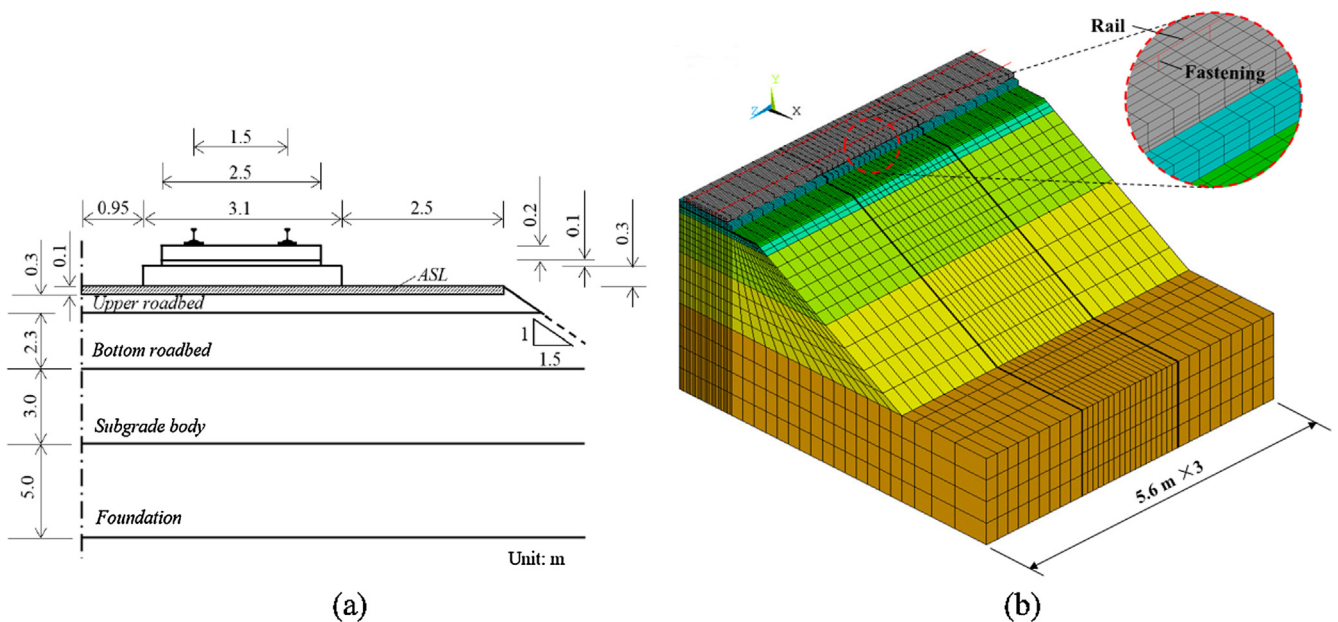


Fig. 3. CRTS III slab track: (a) Cross-section view of structural design, (b) FE model.

the model, are adopted to enforce the constrains at the two ends of the FE slab track model. It was reported [28] that the non-reflective boundary conditions could not only improve the accuracy of simulation results but also save the calculation expenses.

To implement the non-reflective boundary conditions, dampers and springs are attached independently to specific boundaries (i.e., the two ends of the slab track in the longitudinal direction, the bottom and the outer face of foundation) in the normal and tangential directions. The parameters of springs and dampers are calculated according to Eqs. (1) and (2) [29,30]:

$$K_{BT} = \alpha_T \frac{G}{R}, C_{BT} = \rho c_s \tag{1}$$

$$K_{BN} = \alpha_N \frac{G}{R}, C_{BN} = \rho c_p \tag{2}$$

where K_{BT} and K_{BN} are the tangential and normal stiffness coefficients of spring, respectively;

C_{BT} and C_{BN} are the tangential and normal damping coefficient of dampers, respectively;

α_T and α_N are the correction coefficient in tangential and normal directions, respectively;

R is the distance from the vibration source to the boundary;

c_s and c_p are the velocity of the shear-wave and compressive wave, respectively, c_s and c_p are calculated by Eq. (3):

$$c_s = \sqrt{\frac{G}{\rho}}, c_p = \sqrt{\frac{(4/3G + K)}{\rho}} \tag{3}$$

G , K and ρ are the shear modulus, bulk modulus and the mass density of the structure layer, respectively.

The results of numerical simulations showed that the magnitude of the correction coefficient α_T and α_N should fall within a certain range [29]. Otherwise, the calculation accuracy might be negatively affected. The suggested range of α_T is 0.5–1.0, while that of α_N is 1.0–2.0. In this study, the values of α_T and α_N are selected to be 0.67 and 1.33, respectively, and are used for the FE simulations performed.

2.2. Material properties

The material properties of the track components are listed in Table 1. Linear elastic material model is used to describe the constitutive relations of these components, except for the ASL. This is due to the fact that the asphalt concrete is a typical viscoelastic material. Moreover, it was reported [31,32] that the mechanical/dynamic behavior of the asphalt concrete can be easily influenced by the temperature as well as the loading frequency.

Considering the importance of the constitutive relations to the FE analysis, the material model of asphalt concrete is treated with great care. In this study, the generalized Maxwell model in the

Table 1
Material properties [21,33].

Components	Modulus (MPa)	Poisson ratio	Density (kg/m ³)	Damping ratio
Rail	210,000	0.30	7800	0.015
Track slab	350,000	0.20	2500	0.030
Self-compacting concrete	325,000	0.20	2500	0.030
Base plate	325,000	0.20	2500	0.030
Upper roadbed	250	0.30	2200	0.070
Bottom roadbed	200	0.35	2100	0.080
Subgrade	130	0.35	2000	0.090
Foundation	110	0.35	1900	0.100

form of Prony series is adopted for describing the viscoelasticity of asphalt concrete.

To determine the Prony series coefficients, the following experimental procedures are devised:

- (1) The asphalt concrete cores are drilled from the test sections, and are subjected to dynamic modulus test using the universal testing machine;
- (2) The master curve of dynamic modulus (see Fig. 4) was fitted by Williams–Landel–Ferry (WLF) equation [34], utilizing time-temperature superposition principle.
- (3) Based on the master curve fitted, the relaxation modulus can be determined according to the method proposed by Zhang et al. [35]. Finally, the Prony series coefficients are determined by the least square method [36].

Table 2 lists the coefficients of an eleventh order Prony series, which will be used to describe the constitutive relation of the asphalt concrete. Those coefficients determined can be directly imported into ANSYS software for analyzing the dynamic behavior of ASL.

It should be noted that all the analysis in this study was conducted at the recorded temperature of in-situ test, namely 20 °C. The analysis at varying temperatures, which affect the Prony series coefficients of viscoelastic material (herein it refers to asphalt concrete), will be presented in the future work.

2.3. Train load

The high-speed trains operated at test sections are CRH380 (See Fig. 5). The nominal axle load of this kind of high-speed train is 17 t. Thus the load shared by each wheel is set as 85 kN.

In this study, the single-bogie (two wheel-sets) model was adopted to characterize the high-speed train load. Referring to the method documented in the literature [37–39], the wheel-rail contact was simplified as moving wheel load acting on the rail, so as to simulate the impact load of the train wheel. The vehicle effects including vibration and damping were neglected. Fig. 6 shows the schematic graph of moving wheel load (single-bogie load) applied in the FE model, and the specific characteristics are summarized as below:

- (1) The rail is modeled by beam elements, and the length of each beam element is 0.21 m. The rail segment between every two fastening systems is discretized into three beam elements, each rail in the model is discretized to 84 beam elements (85 nodes).

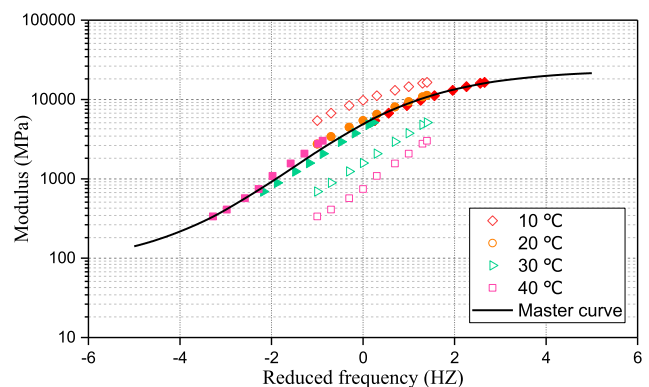


Fig. 4. Master curve of dynamic modulus of asphalt concrete.

Table 2
Prony series coefficients.

Serial number i	Relaxation time τ_i (s)	Prony series g_i	Serial number i	Relaxation time τ_i (s)	Prony series g_i	Instantaneous modulus (MPa)
1	0.000001	0.03192	7	1	0.146179	22,680
2	0.00001	0.055066	8	10	0.068084	
3	0.0001	0.094570	9	100	0.025889	
4	0.001	0.148209	10	1000	0.008865	
5	0.01	0.203485	11	10,000	0.005084	
6	0.1	0.212089				

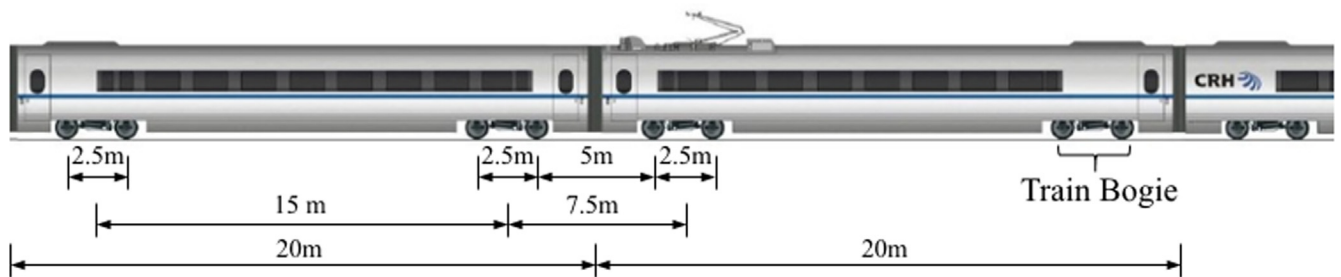


Fig. 5. CRH380 high-speed train (with two carriages).

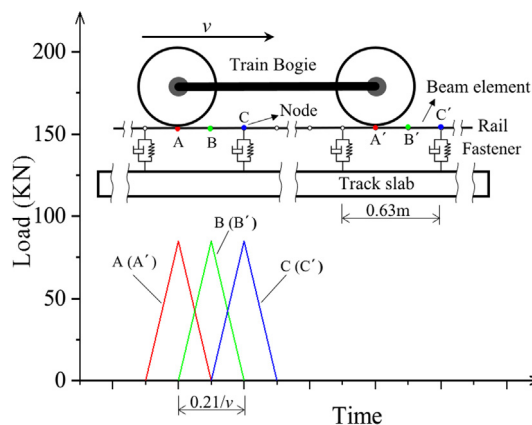


Fig. 6. Schematic graph of moving wheel load applied in the FE model.

- (2) The wheel-rail contact is represented by a concentrated load of which the point of action moves along the rail, so as to simulate the moving train.
- (3) To simulate the moving of action point along the beam element, the concentrated loads are applied on two nodes of the beam element and the amplitude of concentrated load changes over time (See Fig. 6). For example, to simulate the moving of wheel load from node A to node B along the beam element AB, firstly, when the wheel load acts on point A, the concentrated load applied on node A equals to the wheel load (85 kN), and the concentrated load applied on node B equals to zero; then, as the wheel load moves forward, the concentrated load applied on node A starts to decrease gradually, and the concentrated load applied on node B starts to increase gradually, but the sum of the concentrated loads applied on nodes A and B always equals to the wheel load; finally, when the action point moves to point B, the concentrated load applied on node A reduces to zero, and the concentrated load applied on node B increase to 85 kN.
- (4) The calculation time step equals to the ratio of beam element length and the running speed of high-speed train.

Taking the CRH380 as an example, the amplitude of the concentrated load is 85 kN. The nominal running speed V is 350 km/h (97.22 m/s). Thus, the calculation time step is 0.00216 s.

For all the FE simulations performed in this study, the material, mechanical and operational parameters presented in this section are used. Here, the FE simulation refers to the transient analyses that are used to determine the dynamic responses of a structure under the action of the time-dependent load, whenever the inertia and damping effects are important.

3. Model validation

In this section, a general description of the in-situ measurement setup is given first. Then, a detailed comparison between the FE simulated and the filed measured dynamic responses (i.e., acceleration, displacement and stress level) is made. It should be noted that only the dynamic responses in the middle cross-section of the middle slab, which are of great interest, are considered.

3.1. In-situ measurement setup

Fig. 7 shows the setup of the in-situ measurement, which was performed at a 100 m test section (constructed on the Zhengzhou-Xuzhou high-speed line in China) of the slab track incorporating 10-cm thick ASL.

The sensors, including Fiber Bragg Grating (FBG) stress gauge, Charge Coupled Devices (CCD) displacement sensor and piezoresistive accelerometer, were planted in the middle cross-section of the test section (See Fig. 7b). The mechanical properties of the sensors, which are provided by China Geokon Instruments Co., Ltd., are listed in Table 3.

The layout of sensors is illustrated in Fig. 7(a). Using these sensors, the dynamic behavior including displacement, stress, and acceleration of the ASL can be investigated.

The measured data are collected by an in-situ monitoring system (See Fig. 7(c)) powered by a solar panel and designed by China academy of railway sciences. The in-situ measurements could be performed at various speed levels with vary small intervals.

It should be noted that the stress data was not recorded in the in-situ test due to breaking of the stress gage during construction.

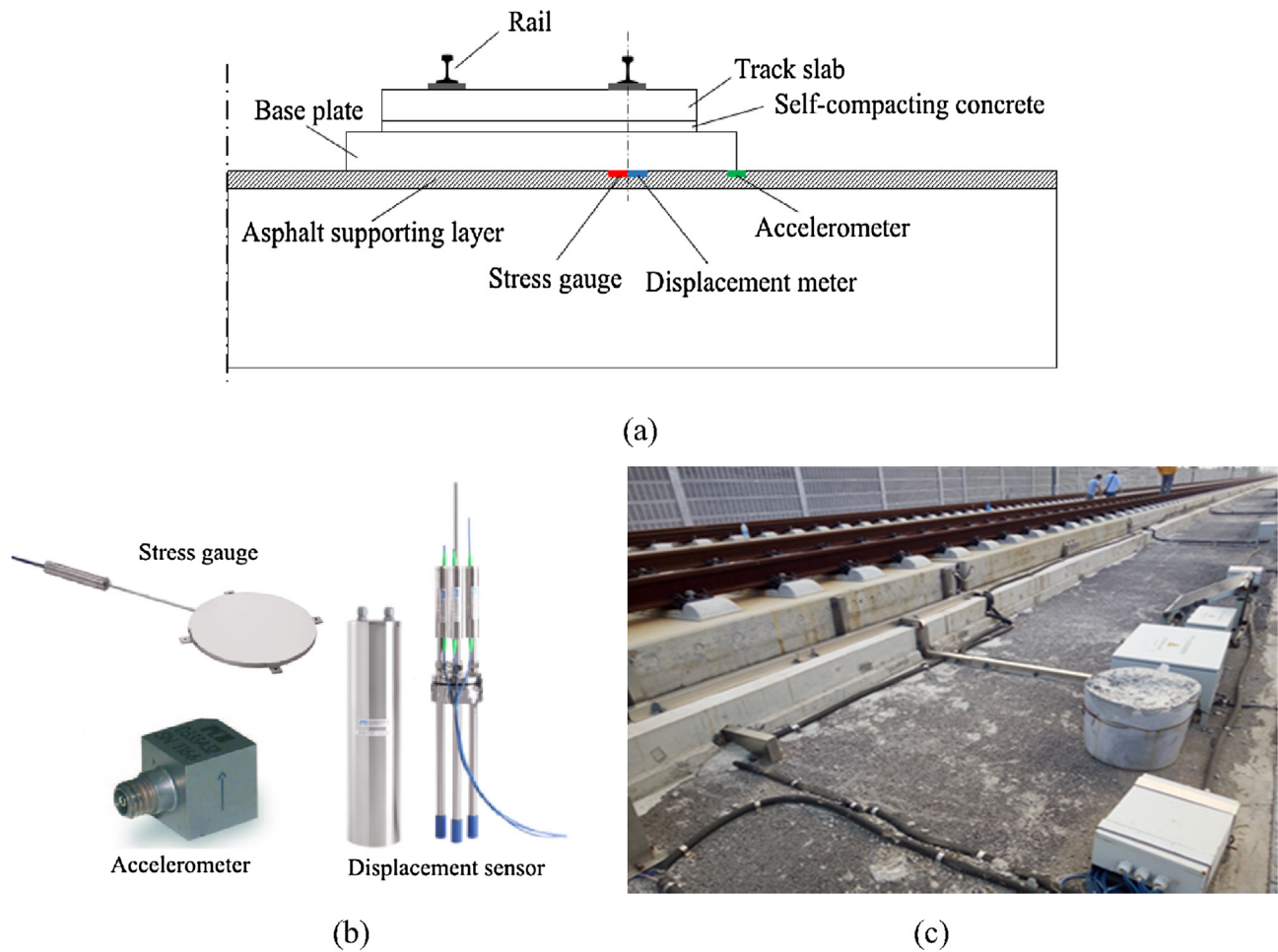


Fig. 7. Setup of in-situ measurement: (a) Schematic graph, (b) Sensors, (c) Monitoring system in the field.

Table 3
Properties of the sensors.

	Range	Accuracy
Stress gauge	0–0.35 MPa	0.1% FS
Displacement sensor	0–50 mm	0.01 mm
Accelerometer	±10 g	0.1 m/s ²

Therefore, only acceleration and dynamic displacement data are available to validate the FE model developed.

3.2. Comparison of measured and simulated results

Fig. 8 presents the comparison of in-situ measurement and simulation results of train-induced acceleration and dynamic displacement on the top of the asphalt supporting layer. For clarity, only the maximum values are presented.

From Fig. 8, it can be seen that, the simulated results act as an upper bound for the acceleration data and a lower bound for the displacement data, but the impact of train speed on the dynamic responses is in agreement with each other, which indicates the effectiveness of the FE model. The value of acceleration is highly dependent on the running speed of the train, and there is a linear relationship between them. Yet, the train speed has little influence on the dynamic displacement. For all the speed levels, the in-situ test results scattered in the range from 0.1 to 0.17 mm, and the simulated values varies from 0.114 to 0.124 mm. The discrepancies can be attributed to the assumptions of train model applied in the

simulation. On one hand, damping of the suspension system was neglected in the moving-wheel model, which results in the increase of simulated dynamic acceleration to some degree; On the other hand, the neglect of rail irregularity, which commonly exists in the newly-operated rail and may amplify the impact of train wheel, contributes to the decrease of dynamic displacement in the simulation.

Although the simulated values have some differences with the average value of in-situ measurement, it is always within the scope of in-situ measurement, and the effect of train speed is correctly reflected. Therefore, it can be concluded that the developed FE model is effective for studying the dynamic behavior of ASL in the slab track system.

4. FE results of dynamic responses of ASL

With the rapid development of non-destructive measuring/monitoring technologies (e.g. the in-situ measurement setup discussed before), nowadays it has become easy to measure the dynamic responses and/or to monitor the health conditions of railway track components at specified test sites. However, due to the high investment cost and the inaccessibility of measuring/monitoring devices to many and/or any test sites, the verified/validated numerical models are much preferred by virtue of their low economic cost and great flexibility.

In this section, using the validated FE model, the dynamic responses of ASL under moving train load are analyzed so as to identify the features of its working environment. To minimize

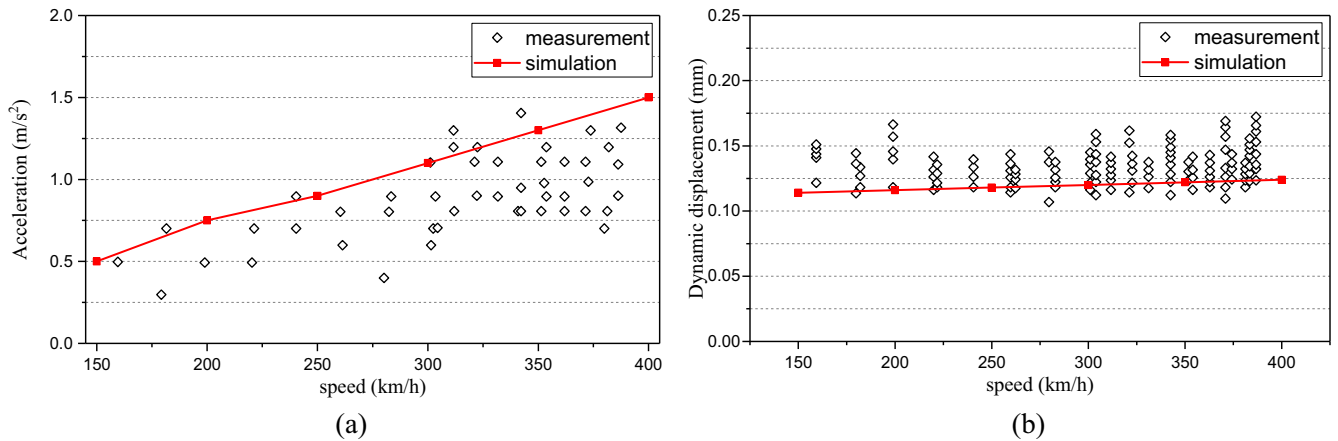


Fig. 8. Comparison of measured and simulated results: (a) Acceleration, (b) Displacement.

the effects of boundary conditions, the simulation results are extracted from the middle cross-section of ASL, and special attention is focused on the variation of dynamic responses in the area exactly underneath the right rail (see Fig. 9).

In addition, for convenience, the directions along the X, Y, and Z axis are defined as lateral, longitudinal, and vertical directions, respectively, as shown in Fig. 9.

4.1. Stress responses on the surface of ASL

Fig. 10 shows the stress responses on the top and bottom surfaces of ASL in the area of interest. It can be seen that the maximum principal stress caused by train passage is the compressive stress on the top surface of ASL, but tensile stress on the bottom surface of ASL. The relative position between train bogie and the middle cross-section at several critical time points are shown in Fig. 11.

During the train passage, the variation trends of the stress responses on the top and bottom surface of ASL are the same. Its amplitudes depends on the relative position of wheel-set, and the time-history curves of bogie approaching and departing are symmetric. All the amplitudes of stresses reach the peak values at the time instants of 0.0853 s and 0.1110 s, when the wheel-set

acts directly above the middle cross-section. When the middle cross-section locates between the two wheel-sets of train bogie, the stresses drop to trough values (0.1 s).

As the bogie is approaching, the longitudinal compressive stress occurs first. It reaches the peak value at 0.0607 s. When the bogie is about 2.4 m away from the middle cross-section, it decreases rapidly, and then changes to be tensile stress, and reaches the maximum value at 0.0853 s. Similarly, as the bogie is departing, the tensile stress decreases rapidly and reaches the peak value at 0.1376 s, when the bogie has departed to the position that is 2.6 m away from the middle cross-section.

It can be seen from Fig. 10 that, on both the top and bottom surface, the tensile stress in the longitudinal direction is larger than that in the lateral direction. The vertical compressive stress and longitudinal tensile stress are dominant on the top and bottom surface of ASL, respectively. Therefore, only these two stress responses need to be considered in the analysis. It should be noted that the asphalt layer is not acting in traditional bending mode, the stresses at the top and bottom of ASL are both tensile stress. Fig. 12 illustrates the stress state of ASL in the slab track system. In the slab track structure system, the asphalt layer is placed underneath the superstructure consists of track slab, self-compacting concrete layer, and base plate. The whole super-structure is very thick and

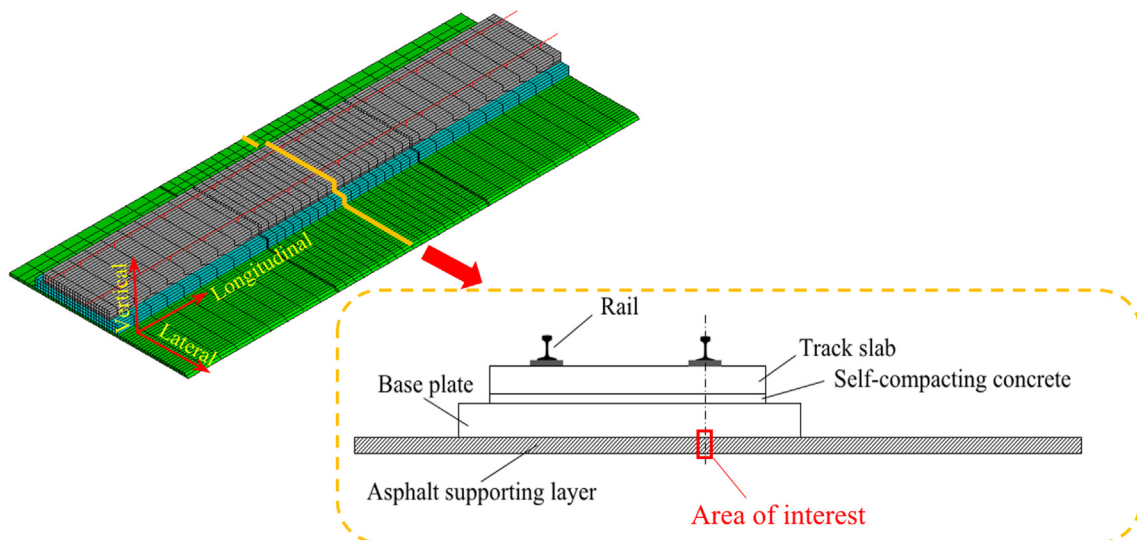


Fig. 9. The area of interest in the middle cross-section of ASL.

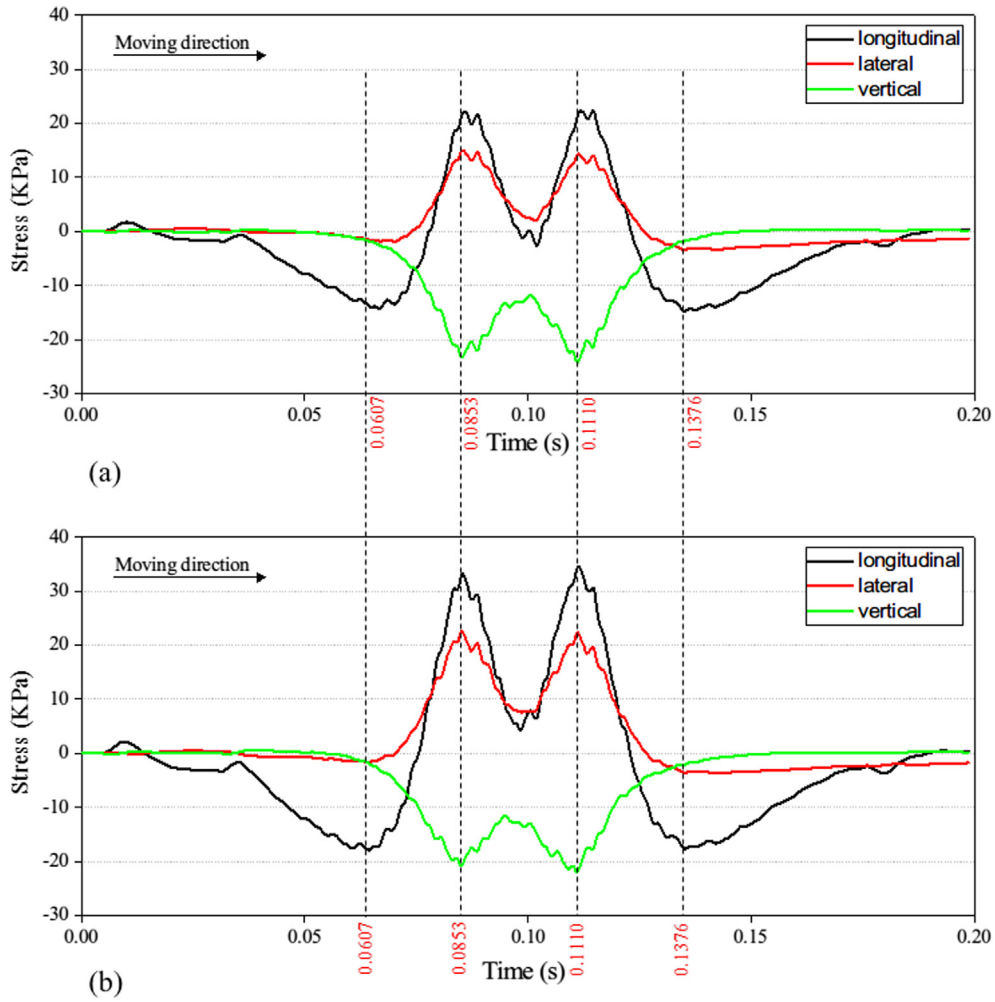


Fig. 10. The variation of stress responses on the top (a) and bottom (b) surface of ASL.

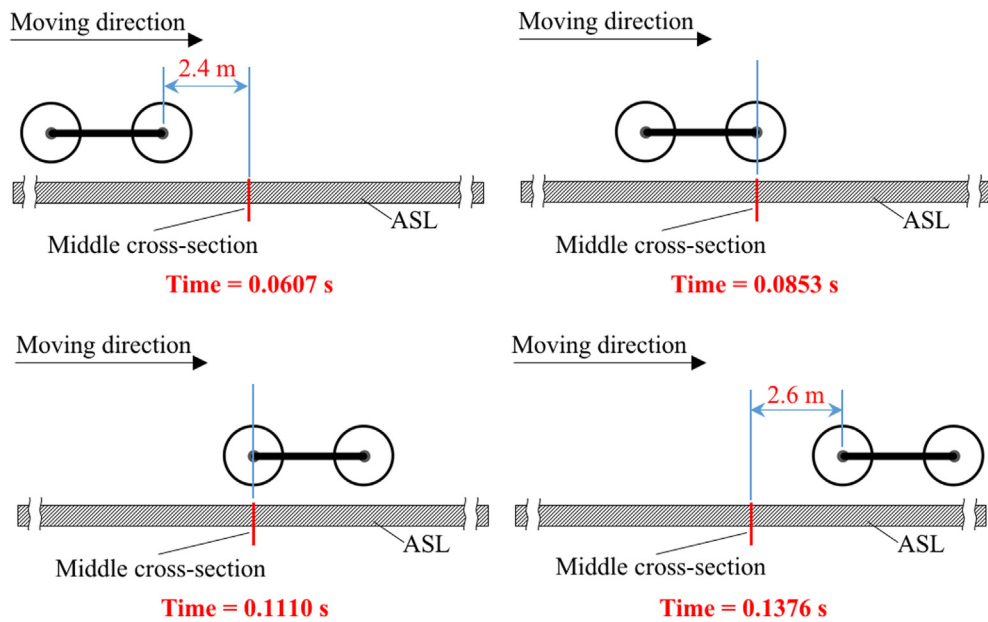


Fig. 11. Schematic graph of the single-bogie movement with respect to the middle cross-section of ASL.

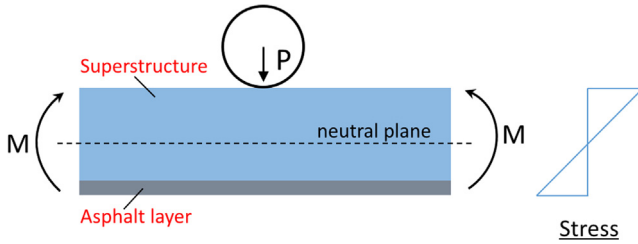


Fig. 12. The stress state of ASL in the slab track system.

has high bending stiffness, it acts like one plate under the train load. The thin asphalt layer is bonded to the bottom face of the base plate and has low bending stiffness, thus the train-induced stresses at the top and bottom of the asphalt layer are all tensile stress.

Fig. 13 shows the variation of shear stresses on the top and bottom of ASL. The shear stress between ASL and adjacent layers is critical to interlayer bonding performance. It can be seen that, during the train passage, large shear stresses occur at both top and bottom surface of ASL. The direction of shear stresses vary with the relative position between wheel-set and the middle cross-section.

As the bogie is approaching the middle cross-section, the shear stress is negative (towards the moving direction of the bogie). The amplitude reaches the maximum value at 0.0791 s, when the bogie is about 0.6 m away from the monitoring cross-section. When the bogie moves across the middle cross-section, the shear stress changes from a negative value to a positive one first, and then it changes to be negative again. Next, as the bogie is departing the middle cross-section, the shear stress changes to be positive, and the amplitude reaches the maximum value at 0.1236 s, when the bogie is 1.2 m away from the monitoring cross section.

Based on the simulation results, it can be concluded that, under moving bogie load, the variation of the stress responses of ASL relies on the position of wheel-set. The reach of the stress responses in ASL is about 7.5 m in the longitudinal direction. The passage of bogie causes shear stress between ASL and adjacent layers, and its direction reverses while the bogie moving across. Therefore, a good bonding between ASL and adjacent layers, especially the base plate, is needed to prevent the potential interlayer sliding.

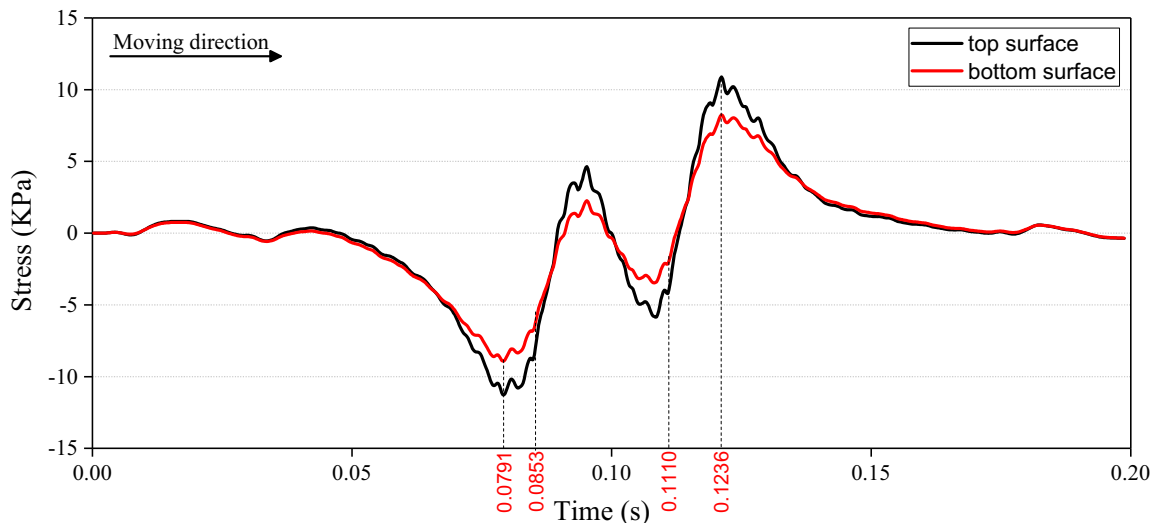


Fig. 13. Variation of shear stresses occurs at the interfaces of base plate-ASL and ASL-upper roadbed.

4.2. Displacement and acceleration responses on the top of ASL

Fig. 14 shows the time-history curve of dynamic displacement and acceleration on the top surface of ASL. Being the same as dynamic stresses, the variation of acceleration mainly hinges on the relative position of wheel-set and the middle cross-section. During the passage of the bogie, the amplitude of acceleration reaches the maximum value twice around 0.0853 s and 0.1110 s, respectively. Also, it starts to increase rapidly at 0.0607 s and drops to a relative low value at 0.1376 s.

However, the variation of vertical displacement depends on the position of the whole bogie. As the bogie is approaching, a positive displacement of small amplitude is caused firstly, and then it changes to be negative and the amplitude increase gradually with the bogie moving closer to the middle cross-section. Next, while the bogie moving across the middle cross section, the dynamic displacement remains at a high amplitude. Finally, as the bogie is departing, the dynamic displacement amplitude decreases gradually.

4.3. Distribution of dynamic responses in ASL

To investigate the lateral distribution of the dynamic responses in the cross section of ASL, the train-induced stress and displacement responses at 0.1 s, when the train bogie moves onto the middle of the second track slab, are shown in Fig. 15.

It can be seen from Fig. 15(b) that, except for the stress concentration exists at the edge of the base plate, the vertical stress on the top of ASL peaks at the positions exactly underneath the wheel-rail contact point, and distributed evenly in other area under the base plate. The shear stress (Fig. 15(c)) occurs in the whole area beneath the base plate, and on two sides of the bogie, the direction of shear stress is opposite. Moreover, a large level of shear stress occurs in the local area around the edge of base plate. On the bottom of ASL, longitudinal stress (Fig. 15(d)) mainly occurs in the area underneath the two wheel-sets, and the amplitudes in other area is very small.

Fig. 15(e) shows the displacement on the top of ASL. The amplitude of displacement decreases gradually as the position getting closer to the line center due to the overlap effect of double-line train load. It is the deformation of roadbed and subgrade that causes the displacement of ASL. The overlapping of double-line train load causes larger pressure in the middle area of roadbed

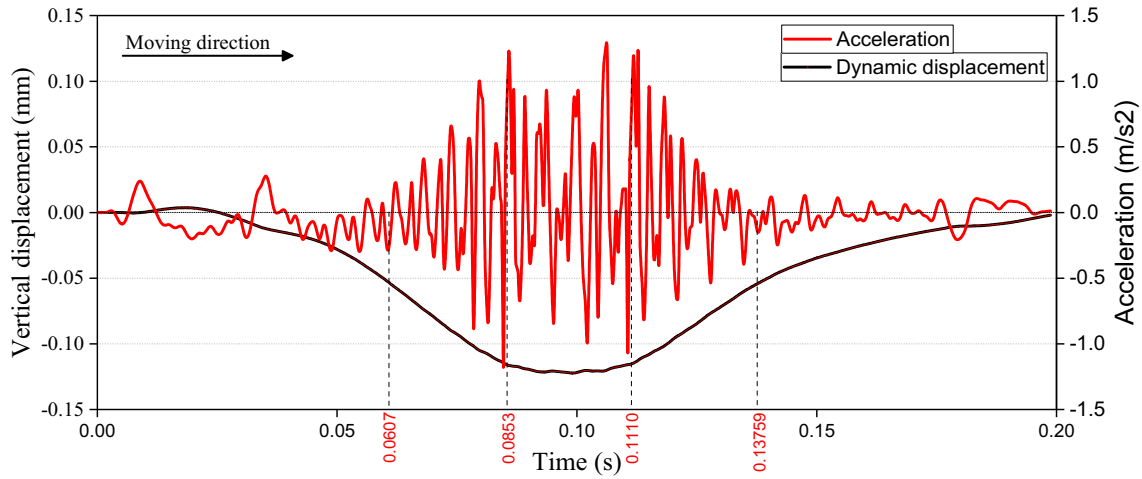


Fig. 14. Dynamic responses on the top surface of ASL: vertical displacement and vertical acceleration.

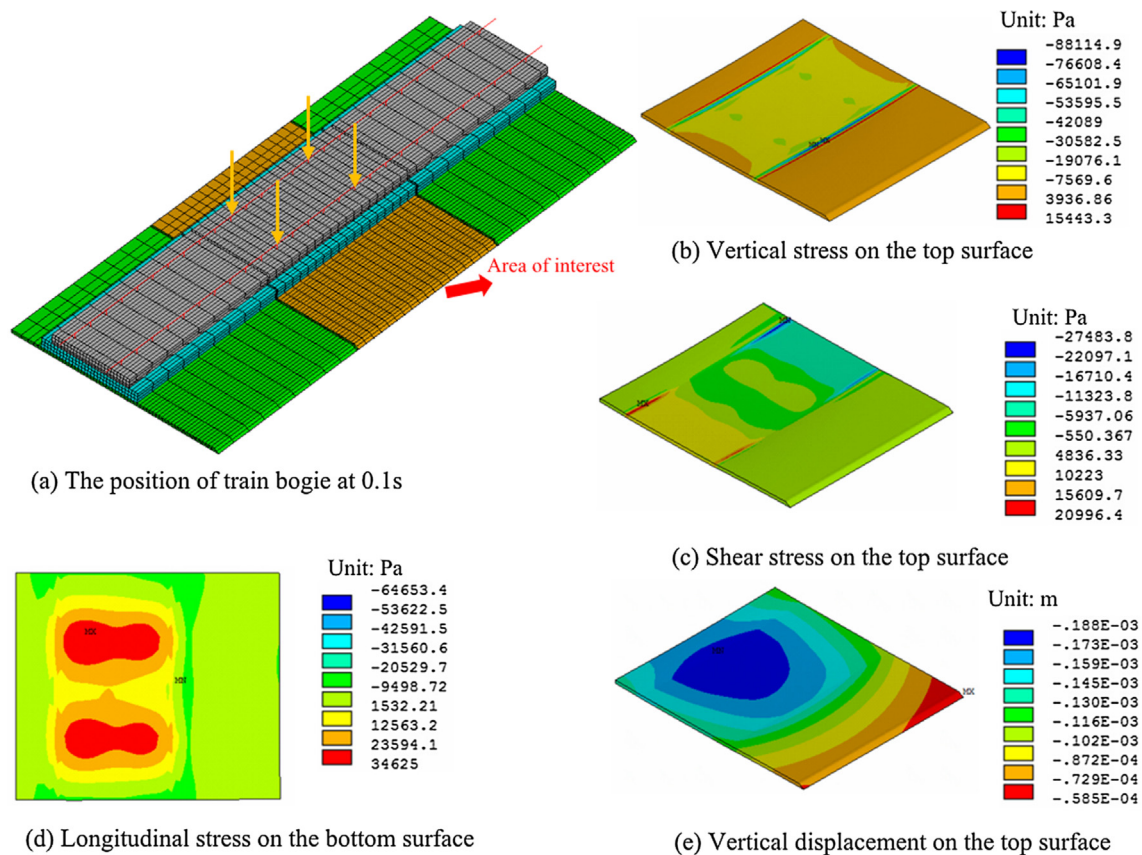


Fig. 15. Distribution of the dynamic responses on the surface of ASL at 0.1 s.

and subgrade, as a result, on the top of ASL, the displacement in the inner side is larger than that in the outer side.

Based on the simulation results, the train-induced dynamic responses in ASL mainly occur in the area beneath the base plate, and they distributed unevenly in the cross-section. For the stress responses, the maximum amplitudes exist at the position beneath the rails. Also, high stress is found in some area on the side of base plate, which should be seriously taken into consideration in the design of ASL. The dynamic response of displacement on the top of ASL mainly comes from the deformation of roadbed and subgrade, which reaches the maximum value in the center area. There-

fore, the carrying capacity of roadbed and subgrade is significantly important to the stability of ASL.

5. Parametric effects of subgrade modulus

In the developed model, the modulus values of subgrade and foundation were defined based on the support condition of the newly built high-speed railway in China, thus, the support condition is very good. However, the varying of soil materials as well as changing of soil water content may affect the support condition

Table 4
Modulus for different subgrade and foundation conditions.

	Good	Medium	Poor
Subgrade modulus (MPa)	130	100	60
Foundation modulus (MPa)	110	80	40

of subgrade and foundation [40]. To consider the effects of degradation of subgrade and foundation support condition, a series simulation were conducted by setting three different subgrade and foundation conditions in the FE model, namely good, medium and poor conditions. The detailed modulus is shown in Table 4 [23,27,33].

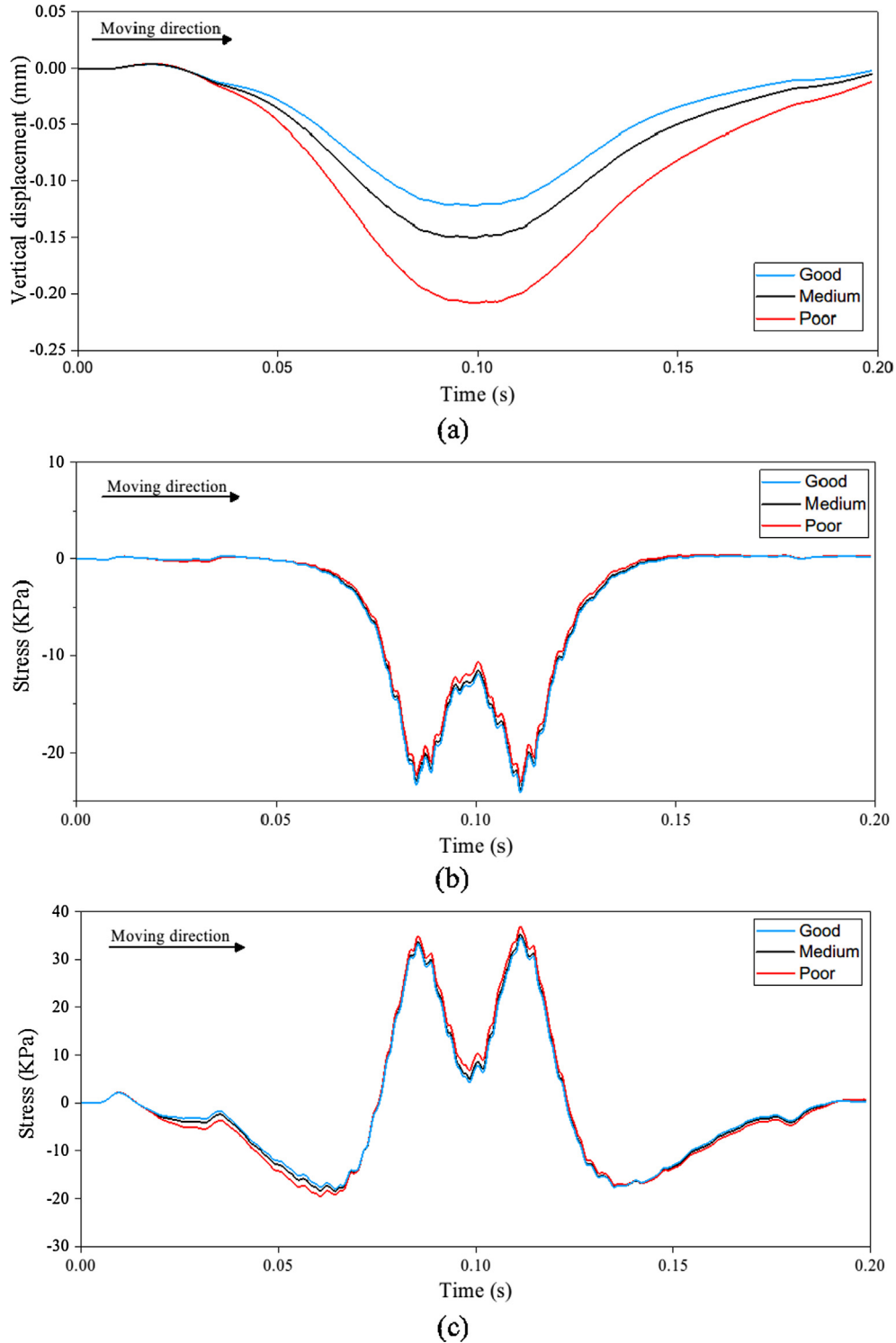


Fig. 16. Effects of degradation subgrade and foundation support condition on the dynamic responses on ASL: (a) the dynamic displacement on the top surface, (b) the vertical compressive stress on the top surface, (c) the longitudinal tensile stress on the bottom surface.

The simulation results are shown in Fig. 16. It can be found that, the degradation of support condition may obviously increase the dynamic displacement on the top of ASL (see Fig. 16(a)), but slightly decrease the vertical compressive stress on the top of ASL (see Fig. 16(b)) and increase the longitudinal tensile stress on the bottom of ASL (see Fig. 16(c)).

The degradation of subgrade and foundation support condition results in larger deformation of subgrade and foundation under train load, thus increase the dynamic displacement at the top of ASL. Also, it may cause larger deflection of superstructure and thereby decrease the vertical compressive stress on the top of ASL and increase the longitudinal tensile stress on the bottom of ASL.

6. Parametric effects of ASL thickness

The thickness of ASL can not only affect the dynamic performance of the vehicle-track interaction but also the construction cost of slab track system. For instance, the level of ride comfort can be affected by the damping properties of the slab track, while the stability and durability of the whole slab track system might be also affected by the thickness of ASL through damage accumulation. Therefore, parametric study on the ASL thickness is necessary to suggest a good (if not optimal) range of thickness so as to increase/promote the use of latest CRTS III slab track system.

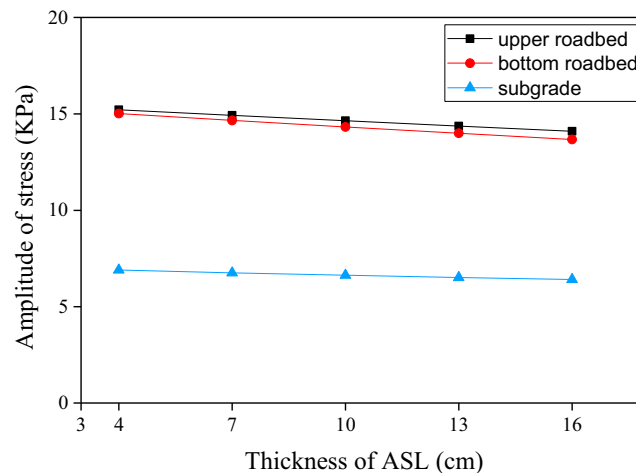
In this section, using the developed FE model, the dynamic responses of five types of slab track structure with varying thicknesses of ASL, namely, 4 cm, 7 cm, 10 cm, 13 cm and 16 cm, are analyzed.

6.1. Dynamic responses of substructure

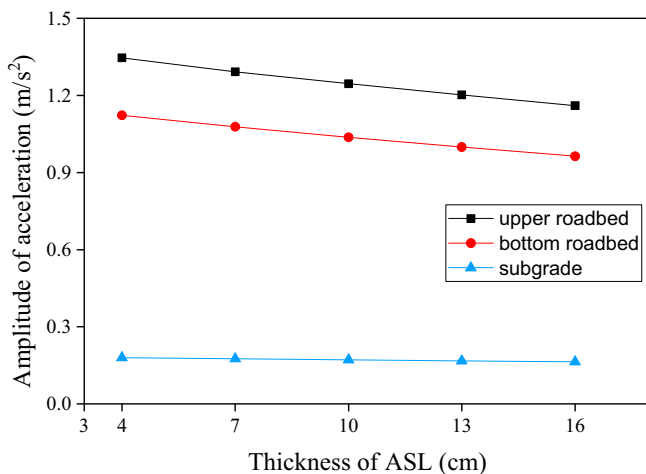
Fig. 17 shows the simulation results of vertical stress, displacement, and acceleration on the top of substructure, including upper roadbed, bottom roadbed, and subgrade, with different thickness of ASL. For clarity, only the maximum amplitudes of them are presented for comparison. It can be seen that the increase of ASL thickness helps to lower the dynamic responses of the substructure, but the effects decrease gradually with the increase of ASL thickness.

6.2. Dynamic responses of baseplate

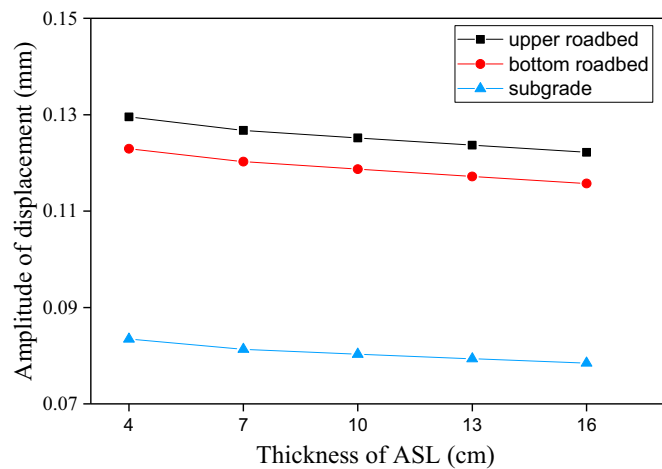
Fig. 18 shows the simulation results of the amplitude of vertical stress and acceleration on the top of base plate. It can be seen that, due to the viscoelasticity of asphalt concrete, the increase of ASL thickness slightly reduced the vibration acceleration of base plate. But, at the same time, the vertical compressive stress on the top of base plate increases as a result of rising supporting stiffness. Therefore, on one hand, increasing of the thickness of ASL provides better damping effects and make more contributions to ride comfort



(a)



(b)



(c)

Fig. 17. The dynamic responses of substructure with varying thickness of ASL: (a) vertical stress, (b) vertical acceleration, (c) vertical displacement.

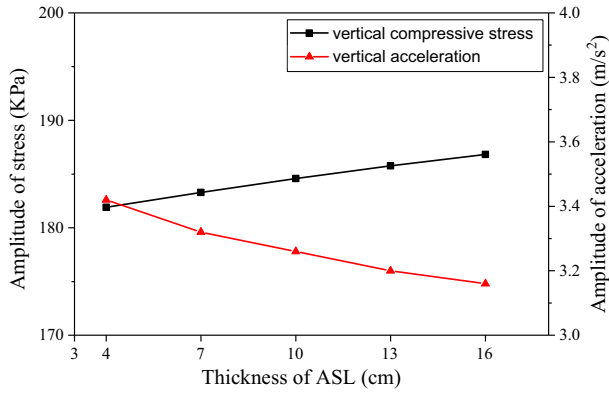


Fig. 18. The amplitude of vertical stress and acceleration on the top of base plate.

and running safety of high-speed train, on the other hand, it increase the amplitude of the vertical stress in base plate.

6.3. Dynamic responses of the ASL

Fig. 19 shows the amplitude of dynamic stresses and displacement of ASL with varying thickness of ASL. As discussed before, the longitudinal tensile stress is dominant on the bottom of the ASL, so only the amplitude of the longitudinal tensile stress at the bottom surface of ASL is shown in Fig. 19(a). It can be seen that, when the thickness of ASL is less than 10 cm, increase of ASL thickness obviously increases the longitudinal tensile stress on the bottom surface of ASL, but the influence turns to be smaller when the ASL is thicker than 13 cm. While, the amplitudes of both vertical compressive stress and dynamic displacement on the top surface of ASL decrease with increase of thickness of ASL, and the decrease rate drops gradually with increasing thickness. Especially for the dynamic displacement, it decreases remarkably when the thickness increase from 4 cm to 7 cm.

Fig. 20 shows the amplitude of shear stresses between ASL and adjacent layers with varying thickness of ASL. It can be seen that the shear stresses increase dramatically with the increase of ASL thickness, and the shear stress in base plate-ASL interface is more sensitive than that in ASL-upper roadbed interface. When the thickness of ASL increases from 4 cm to 16 cm, the shear stress in base plate-ASL interface increases from 8.9 KPa to 12.6 KPa.

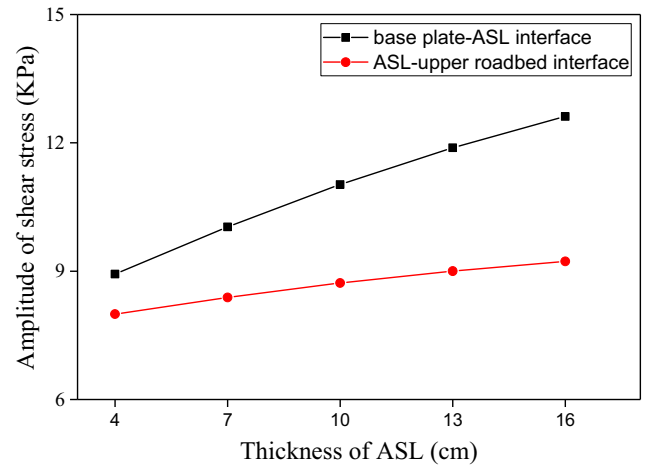


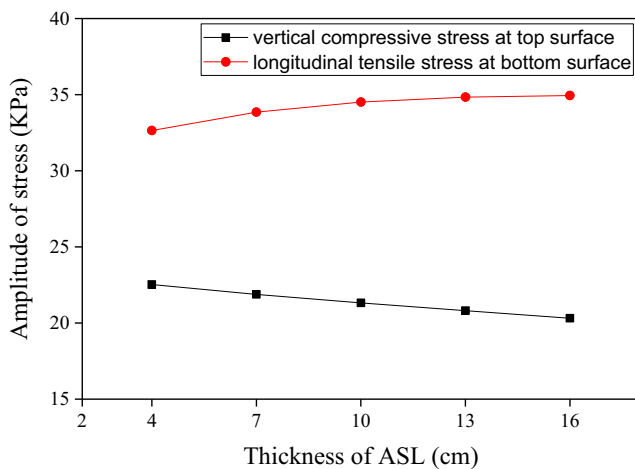
Fig. 20. The amplitude of shear stresses between ASL and adjacent layers with varying thickness of ASL.

In summary, a larger thickness of ASL may reduce the train-induced vertical compressive stress and displacement of ASL, but increase the longitudinal tensile stress and shear stress in ASL. Provided that the vertical compressive stress and displacement are relating to permanent deformation of ASL, and the longitudinal tensile stress and shear stress are critical to fatigue life of ASL. In order to ensure the long term performance of ASL, a moderate thickness of ASL is suggested for use in the slab track system.

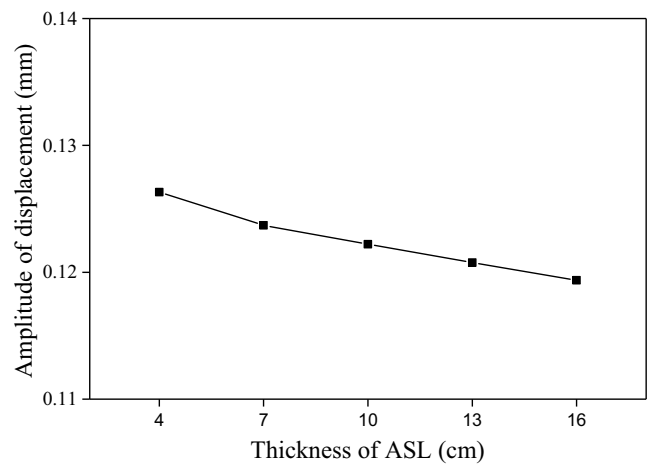
6.4. Discussion on the selection of optimal ASL thickness

Based on the above analysis, the dynamic response of slab track is significantly affected by the thickness of ASL. A thicker ASL can provide better damping property, greater substructure stability, and better ride comfort. But for the sake of durability and stability of ASL itself, a moderate thickness of ASL is preferred.

However, the economic and construction factors should also be seriously considered for the determination of ASL thickness. On one hand, the amount of asphalt concrete will increase linearly with the increase of ASL, as a result, the material cost will be proportional to ASL thickness. On the other hand, the construction of asphalt concrete requires that the paving thickness of single layer



(a)



(b)

Fig. 19. The amplitude of dynamic responses of ASL with varying thickness of asphalt supporting: (a) amplitude of vertical compressive stress and longitudinal tensile stress, and (b) amplitude of dynamic displacement.

be less than 10 cm. The double-layer paving technology will be required if the ASL thickness exceeds 10 cm, which may greatly increase the cost of ASL construction. Synthesizing the dynamic behavior of ASL and economic factors, an optimal thickness range of 7–10 cm is recommended for ASL in CRTS III slab track.

7. Conclusions

The application of ASL in CRTS III slab track was introduced and studied in this paper. A FE model of vehicle and slab track interaction was developed. The accuracy of this model was validated against in-situ measurement. Using the validated FE model, the features of dynamic responses of ASL under moving train load were analyzed. Finally, the parametric effect of ASL thickness on the dynamic responses of superstructure and substructure as well as ASL itself were investigated. Based on the results of the analysis, the following conclusions have been drawn:

- (1) The simplified train load model and non-reflective boundary conditions applied in the FE model works well and can accurately capture the variation of stresses, accelerations, and displacements in slab track system. Prony series can successfully characterize the viscoelasticity of asphalt concrete.
- (2) Although the simulated values have some differences with the average value of in-situ measurement, it is always within the scope of in-situ measurement and the effect of train speed is correctly reflected, which validates the effectiveness of the FE model.
- (3) Under the moving bogie load, the reach of the dynamic responses in ASL is about 7.5 m in the longitudinal direction. A good bonding between ASL and adjacent layers is needed to prevent the potential interlayer sliding.
- (4) The maximum stresses in ASL occur at the position beneath the rails, and the dynamic displacement of ASL is mainly affected by the stiffness of roadbed. The degradation of subgrade and foundation support condition may result in larger deformation of subgrade and foundation under train load, thus increase the dynamic displacement at the top of ASL.
- (5) A thicker ASL can provide better damping property, greater substructure stability, and better ride comfort, and the effects of thickness decreases gradually with the increase of ASL thickness. Considering the economic and construction factors, an optimal thickness range of 7–10 cm is recommended for ASL in CRTS III slab track.

Declaration of Competing Interest

The authors declared that there is no conflict of interest.

Acknowledgment

This project has received funding from the National Natural Science Foundation of China (project number 51778136, 51778140) and the China Scholarship Council. The authors also thank for the help from Dr. Valeri Markine, and support of Railway Engineering section of Delft University of Technology, The Netherlands.

References

- [1] J.G. Rose, R.R. Souleyrette, Hot-mix asphalt (bituminous) railway trackbeds—a global perspective Part I—introduction to asphalt trackbeds and international applications and practices, in: M. Losa, T. Papagiannakis (Eds.), The 3rd International Conference On Transportation Infrastructure, CRC Press, Pisa, Italy, 2014.
- [2] J.G. Rose, R.R. Souleyrette, Hot-mix asphalt (bituminous) railway trackbeds—a global perspective Part II—United States asphalt trackbed applications and practices, in: M. Losa, T. Papagiannakis (Eds.), The 3rd International Conference On Transportation Infrastructure, CRC Press, Pisa, Italy, 2014.
- [3] M. Sol-Sanchez, L. Pirozzolo, F. Moreno-Navarro, M.C. Rubio-Gamez, Advanced characterisation of bituminous sub-ballast for its application in railway tracks: the influence of temperature, *Constr. Build. Mater.* 101 (2015) 338–346.
- [4] P.F. Teixeira, A.L. Pita, P.A. Ferreira, New possibilities to reduce track costs on high-speed lines using a bituminous sub-ballast layer, *Int. J. Pavement Eng.* 11 (4) (2010) 301–307.
- [5] G. D'Angelo, N. Thom, D. Lo Presti, Bitumen stabilized ballast: a potential solution for railway track-bed, *Constr. Build. Mater.* 124 (2016) 118–126.
- [6] J.G. Rose, P.F. Teixeira, N.E. Ridgway, ASME, Utilization of Asphalt/bituminous Layers and Coatings in Railway Trackbeds - A Compendium of International Applications, AMER Soc Mechanical Engineers, New York, 2010.
- [7] P.F. Teixeira, P.A. Ferreira, A.L. Pita, C. Casas, A. Bachiller, The use of bituminous subballast on future high-speed lines in Spain: structural design and economical impact, *Int. J. Railway 2* (1) (2009) 1–7.
- [8] T. Real, C. Hernández, F. Ribes, J.I. Real, Structural and dynamic performance of an asphalt slab track in a sharp curve, *KSCE J. Civ. Eng.* 21 (1) (2016) 315–321.
- [9] M. Sol-Sánchez, G. D'Angelo, Review of the design and maintenance technologies used to decelerate the deterioration of ballasted railway tracks, *Constr. Build. Mater.* 157 (2017) 402–415.
- [10] M. Sol-Sanchez, L. Pirozzolo, F. Moreno-Navarro, M.C. Rubio-Gamez, A study into the mechanical performance of different configurations for the railway track section: a laboratory approach, *Eng. Struct.* 119 (2016) 13–23.
- [11] D. Ramirez, B. Jamel, C.D.A. Sofia, C. Nicolas, R. Alain, B.H. Di, S. Cedric, High-speed ballasted track behavior with sub-ballast bituminous layer, Georail 2014, Marne-la-Vallée, France, 2014.
- [12] G. D'Angelo, S. Bressi, M. Giunta, D. Lo Presti, N. Thom, Novel performance-based technique for predicting maintenance strategy of bitumen stabilised ballast, *Constr. Build. Mater.* 161 (2018) 1–8.
- [13] G. Di Mino, M. Di Liberto, C. Maggiore, S. Noto, A dynamic model of ballasted rail track with bituminous sub-ballast layer, *Proc. - Soc. Behav. Sci.* 53 (2012) 366–378.
- [14] L. Pirozzolo, M. Sol-Sánchez, F. Moreno-Navarro, G. Martínez-Montes, M.C. Rubio-Gómez, Evaluation of bituminous sub-ballast manufactured at low temperatures as an alternative for the construction of more sustainable railway structures, *Materiales de Construcción* 67 (327) (2017) 128.
- [15] P.F. Teixeira, A. Lopez-Pita, C. Casas, A. Bachiller, F. Robuste, Improvements in high-speed ballasted track design: benefits of bituminous subballast layers, *Transp. Res. Rec.* 2006 (1943) 43–49.
- [16] Z. Wang, J. Yang, X. Chen, Mastic asphalt concrete waterproof layer on high-speed railway subgrade in cold regions, Transportation Research Board 94th Annual Meeting, Transportation Research Board, Washington DC, United States, 2015.
- [17] S. Liu, J. Yang, X. Chen, G. Yang, D. Cai, Application of mastic asphalt waterproofing layer in high-speed railway track in cold regions, *Appl. Sci.* 8 (5) (2018) 667.
- [18] E. Yang, K.C.P. Wang, Y. Qiu, Q. Luo, Asphalt concrete for high-speed railway infrastructure and performance comparisons, *J. Mater. Civ. Eng.* 28 (5) (2016).
- [19] F.J. Niu, A.Y. Li, J. Luo, Z.J. Lin, G.A. Yin, M.H. Liu, H. Zheng, H. Liu, Soil moisture, ground temperatures, and deformation of a high-speed railway embankment in Northeast China, *Cold Reg. Sci. Tech.* 133 (2017) 7–14.
- [20] S. Liu, J. Yang, X. Chen, M. Wang, W. Zhou, Design of asphalt waterproofing layer for high-speed railway subgrade: a case study in Heilongjiang Province, China, Transportation Research Board 96th Annual Meeting, Transportation Research Board, Washington DC, United States, 2017.
- [21] T. Xin, Q. Zhang, L. Gao, L. Zhao, J. Qu, Dynamic effects and structure optimization of damping layers of CRTSIIIslab ballastless track for high speed railway, *China Railw. Sci.* 37 (5) (2016) 1–7.
- [22] G.C. Long, H. Liu, K.L. Ma, Y.J. Xie, W.G. Li, Development of high-performance self-compacting concrete applied as the filling layer of high-speed railway, *J. Mater. Civ. Eng.* 30 (2) (2018) 10.
- [23] B. Wu, K. Zhu, Z. Zeng, Z. Yu, W. Wei, Experimental study on the mechanical characteristics of CRTS III slab ballastless track under train load, *J. Rail Way Sci. Eng.* 13 (7) (2016) 1229–1233.
- [24] Y.W. Ma, A.A. Mashal, V.L. Markine, Modelling and experimental validation of dynamic impact in 1:9 railway crossing panel, *Tribol. Int.* 118 (2018) 208–226.
- [25] Y. Momoya, T. Horiike, K. Ando, Development of solid bed track on asphalt pavement, *Quart. Rep. RTRI* 43 (3) (2002) 113–118.
- [26] A. Inc, Ansys Release 17.1, Mechanical Applications Theory Reference, 2016.
- [27] C.N.R. Administration, Code for Design of High Speed Railway of China, Beijing, China, 2014.
- [28] G.X. Chen, D.D. Jin, J. Zhu, J. Shi, X.J. Li, Nonlinear analysis on seismic site response of Fuzhou Basin, China, *Bull. Seismol. Soc. Amer.* 105 (2A) (2015) 928–949.
- [29] L. Jingbo, G. Yin, D. Yixin, Consistent viscous-spring artificial boundaries and viscous-spring boundary elements, *Chin. J. Geotech. Eng.* 28 (9) (2006) 1070–1075.
- [30] G.U. Yin, L.L.U. Jingbo, D.U. Yixin, 3D consistent viscous-spring artificial boundary and viscous-spring boundary element, *Eng. Mech.* 24 (12) (2007) 31–37.
- [31] Y. Ali, M. Irfan, S. Ahmed, S. Khanzada, T. Mahmood, Investigation of factors affecting dynamic modulus and phase angle of various asphalt concrete mixtures, *Mater. Struct.* 49 (3) (2015) 857–868.

- [32] H.R. Zhu, L. Sun, J. Yang, Z.W. Chen, W.J. Gu, Developing master curves and predicting dynamic modulus of polymer-modified asphalt mixtures, *J. Mater. Civ. Eng.* 23 (2) (2011) 131–137.
- [33] G. Yang, L. Gao, X. Liu, W. Zhao, Research on division standard of subgrade frost heaving for CRTS III slab track based on dynamic analysis, *J. China Railw. Soc.* 39 (10) (2017) 110–117.
- [34] J.D. Ferry, L.D. Grandine, E.R. Fitzgerald, The relaxation distribution function of polyisobutylene in the transition from rubber-like to glass-like behavior, *J. Appl. Phys.* 24 (7) (1953) 911–916.
- [35] Y.Q. Zhang, B. Birgisson, R.L. Lytton, Weak form equation-based finite-element modeling of viscoelastic asphalt mixtures, *J. Mater. Civ. Eng.* 28 (2) (2016) 13.
- [36] Z.J. Dong, X.Y. Ma, Analytical solutions of asphalt pavement responses under moving loads with arbitrary non-uniform tire contact pressure and irregular tire imprint, *Road Mater. Pavem. Des.* 19 (8) (2018) 1887–1903.
- [37] L. Hall, Simulations and analyses of train-induced ground vibrations in finite element models, *Soil Dyn. Earthq. Eng.* 23 (5) (2003) 403–413.
- [38] H.G. Jiang, X.C. Bian, C. Cheng, Y.M. Chen, R.P. Chen, Simulating train moving loads in physical model testing of railway infrastructure and its numerical calibration, *Acta Geotech.* 11 (2) (2016) 231–242.
- [39] H. Jiang, X. Bian, Y. Chen, J. Jiang, Full-scale accelerated testing for simulation of train moving loads in track-subgrade system of high-speed railways, *China Civil Eng. J.* 48 (9) (2015) 85–95.
- [40] Y. Guo, W.M. Zhai, Long-term prediction of track geometry degradation in high-speed vehicle-ballastless track system due to differential subgrade settlement, *Soil Dyn. Earthq. Eng.* 113 (2018) 1–11.